Supplementary information for Alignment of semiconducting graphene nanoribbons on vicinal Ge(001)

Robert M. Jacobberger, Ellen A. Murray, Matthieu Fortin-Deschênes, Florian Göltl, Wyatt A. Behn, Zachary J. Krebs, Pierre L. Levesque, Donald E. Savage, Charles Smoot, Max G. Lagally, Patrick Desjardins, Richard Martel, Victor Brar, Oussama Moutanabbir, Manos Mavrikakis, Michael S. Arnold*

DFT calculations. DFT calculations are performed using a plane wave basis set and the projector augmented wave method (PAW)[1, 2] as implemented in the Vienna Ab-initio Simulation Package (VASP).[3, 4] Exchange-correlation interactions are treated using the generalized gradient approximation (GGA) in the parameterization of Perdew, Burke, and Ernzerhof (PBE).[5] Van der Waals forces are modeled with DFT-D2 dispersion corrections[6] and gamma-point-only k-point settings are utilized.[7] The electron wave function is expanded in a plane-wave basis with truncated kinetic energy cutoff of 400 eV. Calculations are performed using two Ge lattice constants: (1) the calculated bulk lattice constant of 5.67 Å, referred to as "relaxed" in the main text, and (2) an expanded lattice constant of 6.04 Å, referred to as "strained" in the main text, to eliminate strain in the graphene lattice along the length of the ribbon, which has a calculated bulk C–C bond distance of 1.42 Å. Ge unit cells are modeled using a supercell with eight layers, in which the top four layers are allowed to relax and the bottom four layers are fixed at either of the lattice constants described above, and range from 16 × 24 Å^2 to 24 × 37 Å^2 to accommodate the surface miscut and minimize interactions of ribbons between periodic unit cells. Periodic images in the z-direction are separated by at least 14 Å of vacuum.

Phase diagrams for H coverage of Ge are constructed by calculating the grand potential (Ω) of a Ge(001)-0° surface ranging from 1/16th monolayer (ML) of H to 1 ML of H (where 1 ML of H is defined as one H atom per one surface Ge atom) exposed to varying pressures of H_2 (Fig. S10a,b).[8, 9] The grand potential (Ω) for each coverage is defined as $\Omega = E_{slab+H} - E_{slab} - N_H{*}\mu_H$, where E_{slab+H} is the total energy of the slab and the adsorbed H, E_{slab} is the total energy of the clean Ge slab, N_H is the total number of H atoms, and μ_H is the chemical potential of H. The chemical potential of H_2 in the gas phase is calculated by $\mu_{H_2} = k_B{*}T{*}\ln(P_{H_2}/P_o) + E_{H_2} + H_{H_2} - H_{H_2o} - T{*}S_{H_2}$, where k_B is the Boltzmann constant, T is temperature, P_{H_2} is the partial pressure of H_2, P_o is the reference pressure of 1 atm, E_{H_2} is the total energy of H_2 in the gas phase determined by DFT, H_{H_2} is the enthalpy of H_2, H_{H_2o} is found in the NIST JANAF tables for H_2,[10] and S_{H_2} is the entropy of H_2 in the gas phase. We assume $H_2(g) \leftrightarrow 2H^*$ is at equilibrium where * signifies that H is adsorbed on the Ge surface. Thus, the chemical potential of H on Ge(001)-0° is described as $\mu_H = 1/2\mu_{H_2}$. At temperatures at which graphene is grown (~ 1183 K), 1/16th ML of H is the most stable coverage by at least ~80 kJ mol^{-1} at all P_{H_2} (Fig. S10c-f). Thus, all Ge surfaces are modeled without H passivation in subsequent calculations.

Phase diagrams for nanoribbons (Fig. 5e, Fig. S11e and S12) are constructed by calculating the grand potential (Ω) of $N = 13$ armchair graphene nanoribbons (where N is the number of C atoms along the zigzag chain that spans the ribbon width) that are ~ 1.5 nm wide on Ge(001)- 9º exposed to a gas phase with partial pressure of CH_4 (P_{CH_4}) of 0.0067 atm and varying P_{H_2}.[8, 9] The grand potential is defined as $\Omega = E_{slab+ribbon} - E_{slab} - N_C{*}\mu_C - N_H{*}\mu_H$, where $E_{slab+ribbon}$ is the total energy of the slab and the ribbon, E_{slab} is the total energy of the clean Ge slab, N_i is the total number of i atoms in a ribbon, and μ_i is the chemical potential of atom i. The chemical potential of CH_4 and H_2 in the gas phase are calculated by $\mu_j = k_B{*}T{*}\ln(P_j/P_o) + E_j + H_j - H_{jo} - T{*}S_j$, where k_B is the Boltzmann constant, T is the temperature, P_j is the partial pressure of species j, P_o is the reference pressure of 1 atm, E_j is the total energy of species j in the gas phase determined by DFT, H_j is the enthalpy of species j, H_{jo} is found in the NIST JANAF tables for species j,[10] and S_i is the entropy of species j in the gas phase. We assume the following reactions are at equilibrium: $H_2(g) \leftrightarrow 2H^*$ and $CH_4(g) \leftrightarrow C^* + 4H^*$, where * signifies that a species is adsorbed on the Ge surface. Therefore, the

chemical potential of H and C atoms on the Ge surface are described as $\mu_H = 1/2\mu_{H_2}$ and $\mu_C = \mu_{CH_4} - 4\mu_{H_2}$, respectively.

The energy difference between ribbons with their downhill edge pinned and uphill edge pinned to Ge(001)-9º are calculated by comparing the total energy per edge C atom that forms a covalent bond with the Ge surface in each unit cell. Relative energies of graphene nanoribbons and Ge slabs are calculated by performing single-point calculations on the ribbon with the slab removed and on the slab with the ribbon removed, respectively.

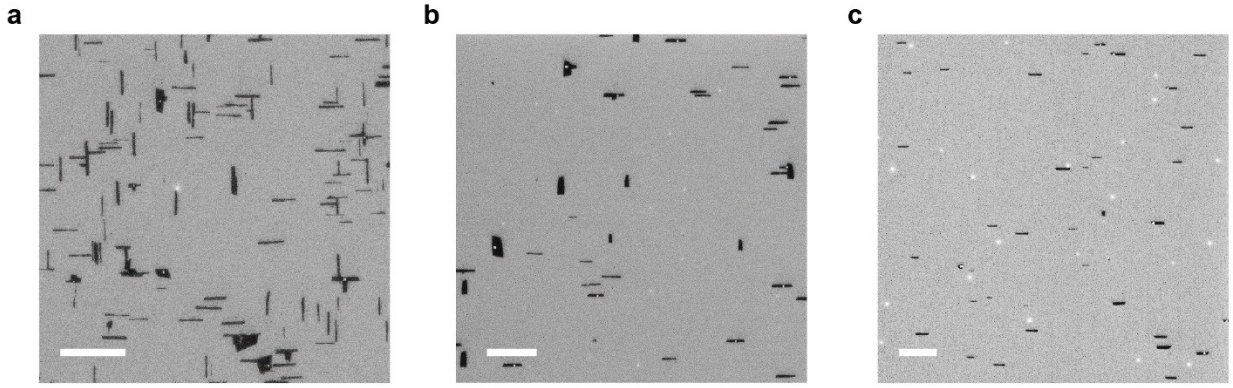

Fig. S1. (a-c) SEM images of graphene grown on Ge(001)-0° (a), Ge(001)-6° (b), and Ge(001)-9° (c). Images of ribbons synthesized using this growth condition are used to characterize alignment, width, length, and aspect ratio in Fig. 1g-j, respectively. Particles are likely due to surface contaminants that are present on the as-purchased Ge wafers. Scale bars are 2 μm.

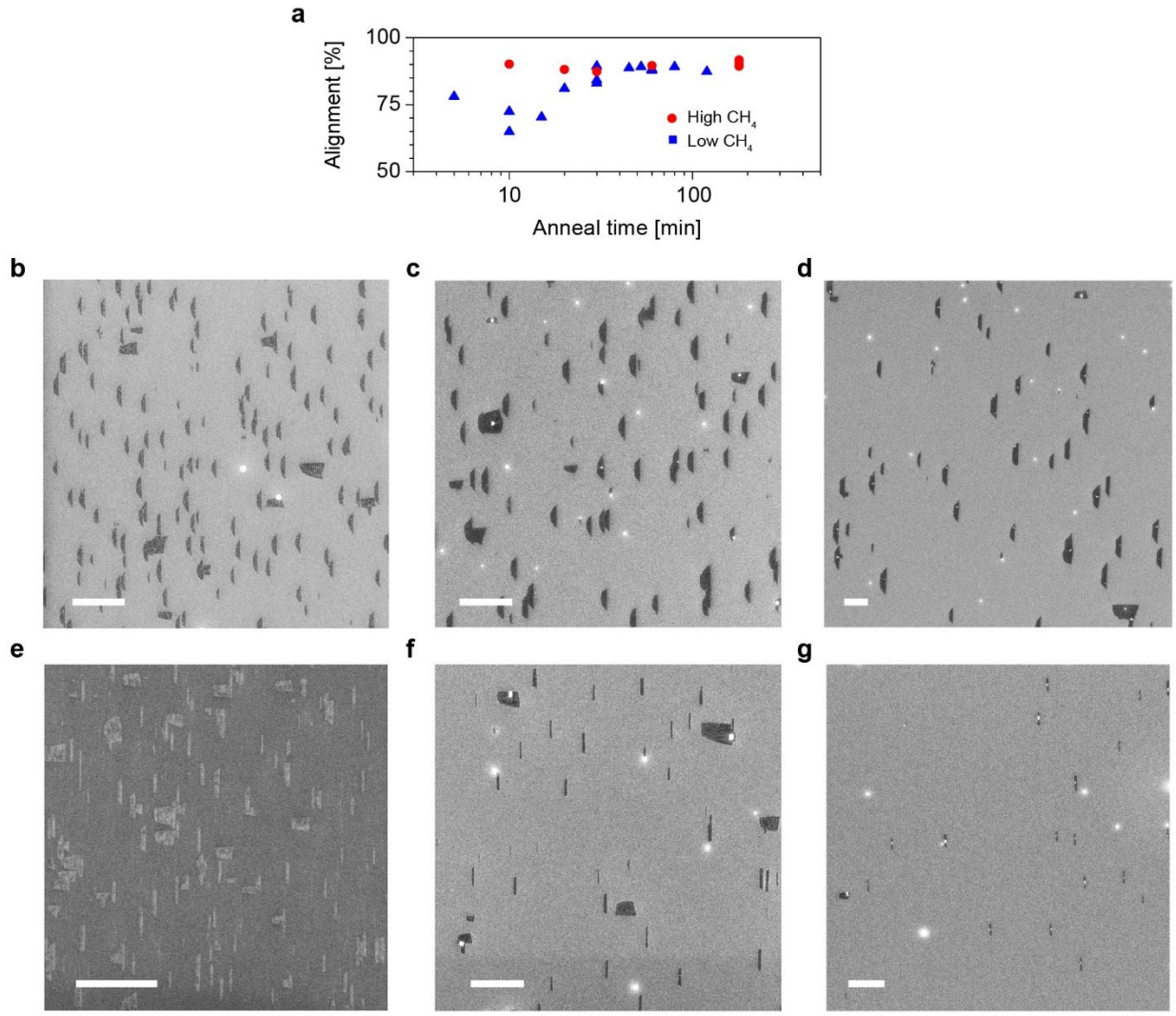

Fig. S2. Effect of pre-growth anneal time on ribbon alignment. (a) Plot of alignment versus anneal time for growth using 4.6 (red circles) and 2.8 (blue triangles) sccm of CH_4 on Ge(001)-9°. (b-g) SEM images of graphene crystals grown using 4.6 (b-d) and 2.8 (e-g) sccm of CH_4 and anneal time of 10 (a), 20 (b), 60 (c), 10 (d), 30 (e), and 45 (g) min. Scale bars are 500 nm in b,e and 1 μm in c,d,f,g. Pre-growth anneal time affects Ge surface topography,[11] which in turn determines the Ge sites available for graphene nucleation, and CH_4 concentration affects feedstock chemical potential, which in turn impacts the type of graphene crystals formed.[12] Characterization of the graphene nucleation sites is beyond the scope of this work. Nonetheless, it is clear that aligned ribbons preferentially nucleate when anneal time is long or CH_4 concentration is high.

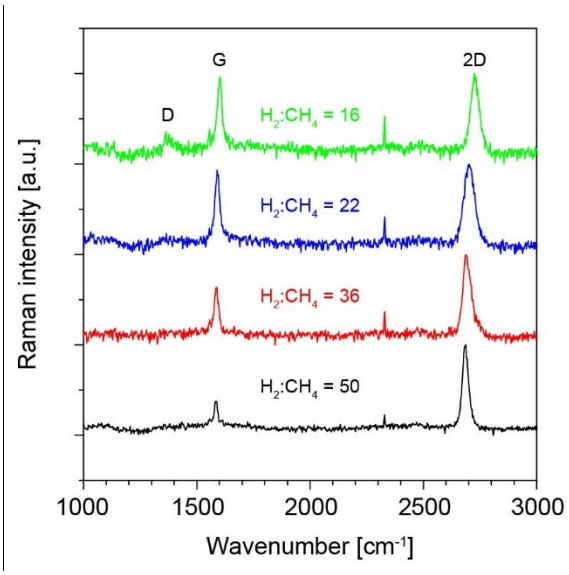

Fig. S3. Raman spectroscopy of single-layer graphene grown on Ge(001)-9° using the same H_2:CH_4 used in Fig. 2, S4, and S5 of 50 (black), 36 (red), 22 (blue), and 16 (green). Each spectrum is the average of at least 25 spectra obtained at different locations on the sample surface. Spectra are normalized to the intensity of the 2D band at ~2700 cm^{-1}.

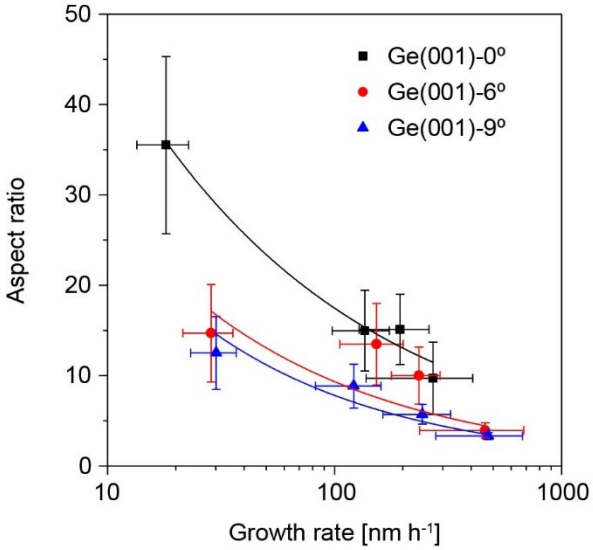

Fig. S4. Effect of growth rate on nanoribbon aspect ratio. Aspect ratio of graphene nanoribbons with lengths of 200–600 nm grown on Ge(001)-0° (black squares), Ge(001)-6° (red circles), and Ge(001)-9° (blue triangles) plotted against growth rate in the direction of the ribbon length. x and y error bars are one standard deviation. Trend lines are added to highlight the decreasing aspect ratio with increasing growth rate on each surface. We define growth rate in the length direction to be $l/(2t)$, where l is crystal length and t is growth time. This formula does not account for the incubation time required to form stable nuclei, during which graphene does not grow. However, we have found this incubation time is significantly less than the total growth time used in our experiments (see Fig. S6), and therefore its effect on the calculated growth rate is relatively small (< 10%).[11]

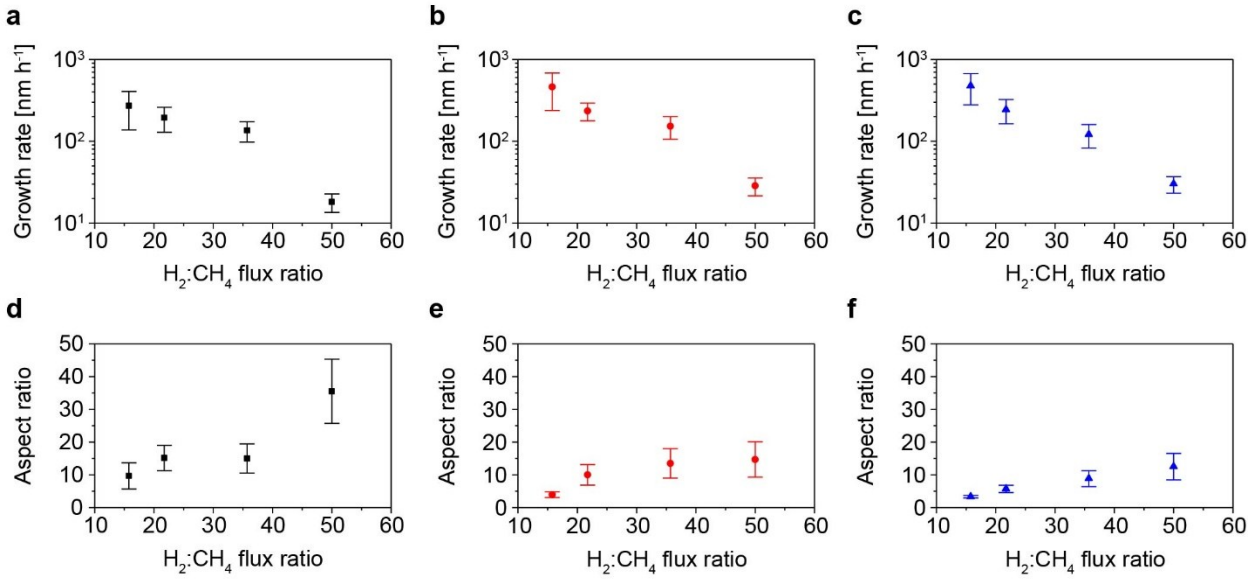

Fig. S5. Effect of H_2:CH_4 on growth rate and aspect ratio. (a-f) Plot of growth rate (a-c) and aspect ratio (d-f) versus H_2:CH_4 on Ge(001)-0° (a,d), Ge(001)-6° (b,e), and Ge(001)-9° (c,f).

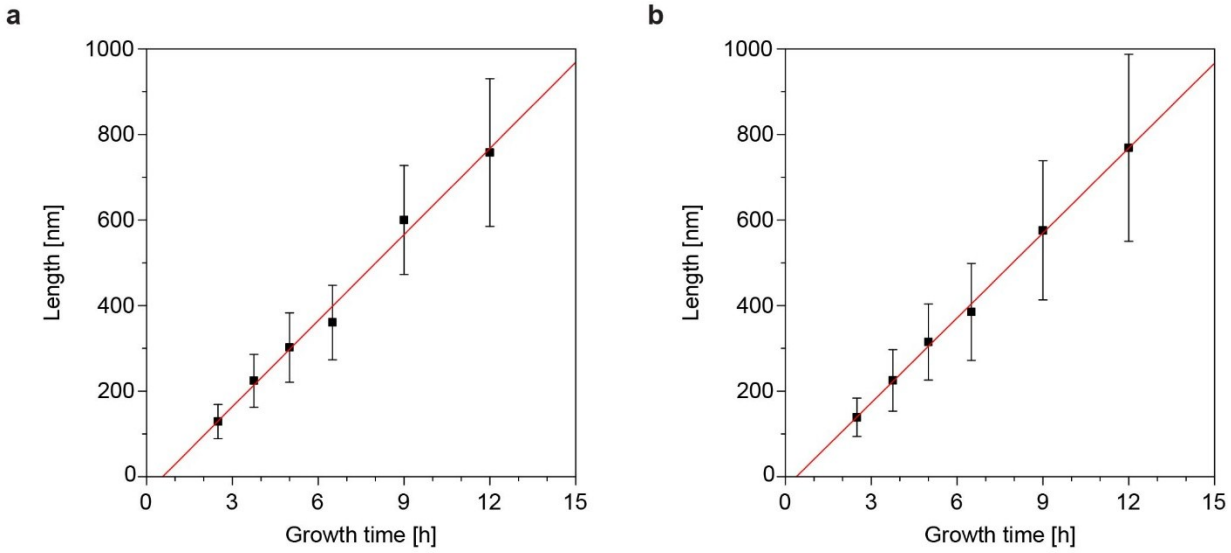

Fig. S6. Effect of growth time on ribbon length. (a-b) Plot of ribbon length versus growth time on Ge(001)-9° (a) and Ge(001)-6° (b) for samples grown at 910 °C with a flow of 200 sccm of Ar, 100 sccm of H_2, and 2.0 sccm of CH_4. The extracted incubation time for nucleation is ~0.5 h on both surfaces. In comparison, the growth time used to determine growth rate in Fig. S4 and S5a-c is 6 h. The incubation time, therefore, may increase the calculated growth rate by < 10%.

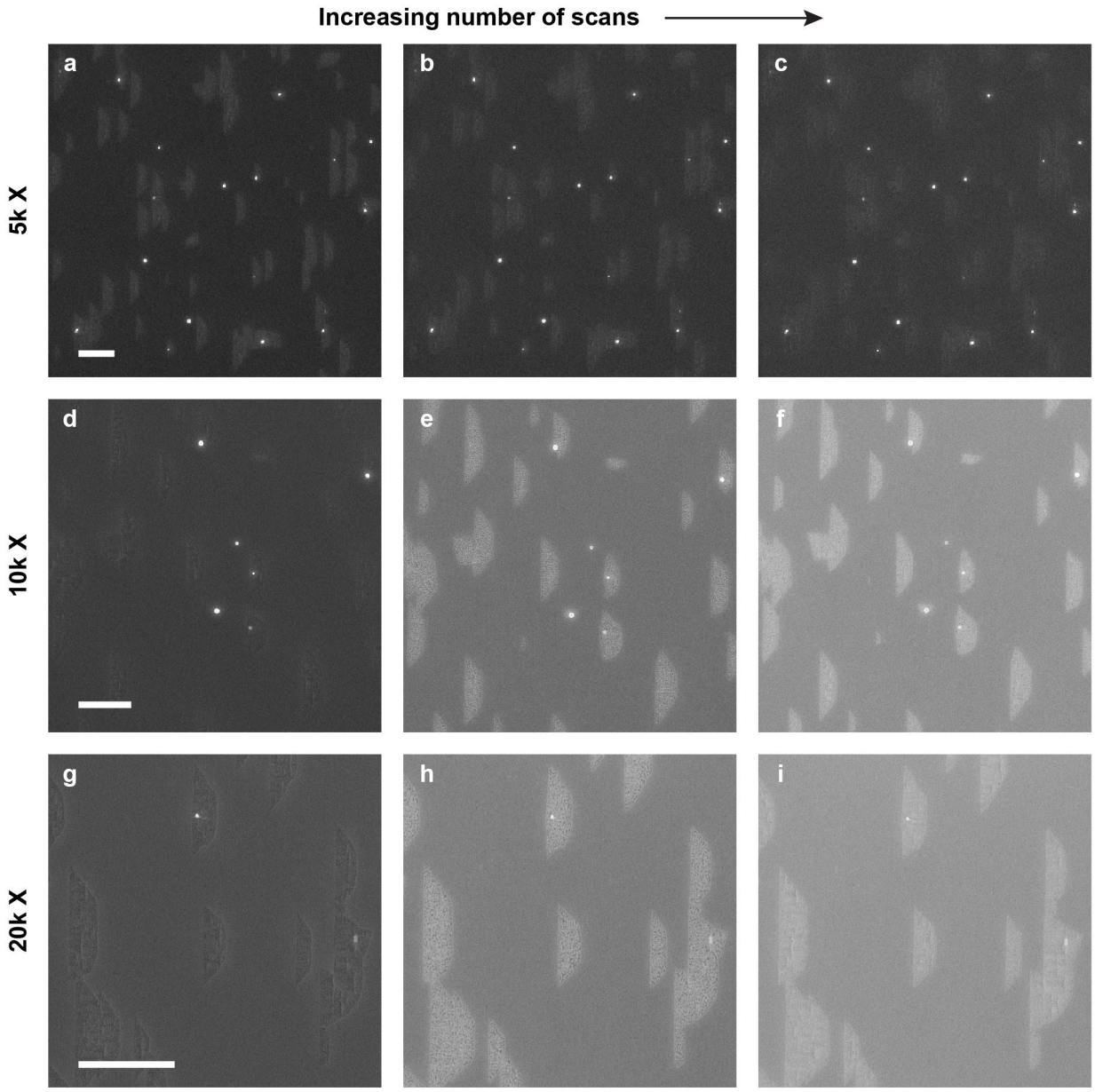

Fig. S7. Effect of magnification and number of scans on SEM contrast after exposure of the sample to air for 0 h. Representative SEM images of graphene on Ge(001)-9° at 5k (top), 10k (middle), and 20k (bottom) magnification factor with increasing number of scans (left to right). Number of scans in a-i is 1, 2, 3, 1, 5, 9, 1, 2, and 3, respectively. All images are obtained using the same brightness and contrast. Scale bars are 1 μm. At each magnification factor, graphene appears lighter than Ge after 1 scan. As the number of scans increases, graphene still appears lighter than Ge, but the contrast is enhanced.

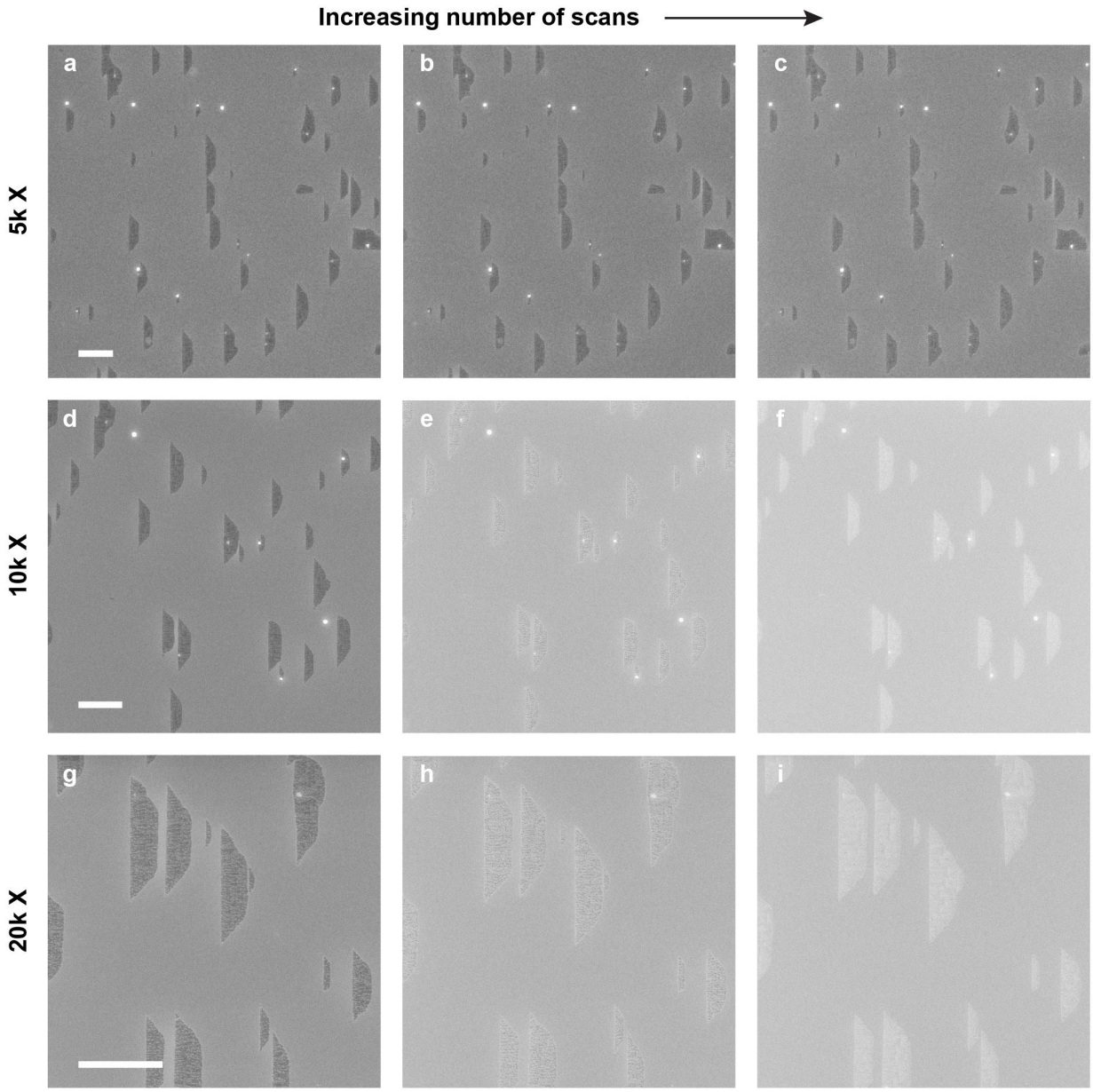

Fig. S8. Effect of magnification and number of scans on SEM contrast after exposure of the sample to air for 32 h. Representative SEM images of graphene on Ge(001)-9° at 5k (top), 10k (middle), and 20k (bottom) magnification with increasing number of scans (left to right). Number of scans in a-i is 1, 4, 6, 1, 5, 9, 1, 2, and 3, respectively. All images are obtained using the same brightness and contrast. Scale bars are 1 μm. At each magnification factor, graphene appears darker than Ge after 1 scan. Conversely, graphene appears lighter than Ge after 1 scan on samples that are exposed to air for 0 h (Fig. S7a,d,g) instead of 32 h (Fig. S8a,d,g), indicating that increasing the air exposure time can cause contrast reversal. Contrast reversal upon exposure to air is likely due to oxidation of the Ge surface. As the number of scans increases in Fig. S8, contrast reverses and graphene appears lighter than Ge, which is likely due to deposition of amorphous carbon upon sample exposure to the electron beam.

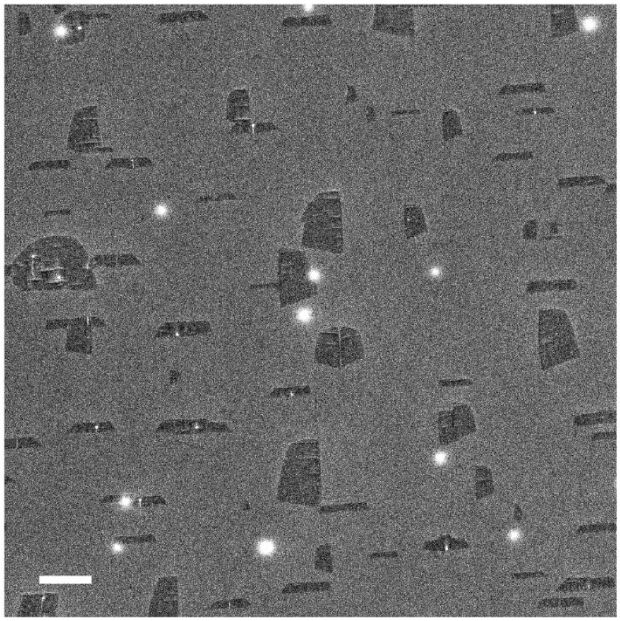

Fig. S9. SEM image of graphene crystals on Ge(001)-9° used for LEEM and LEED studies in Fig. 3a,b. Scale bar is 1 μm.

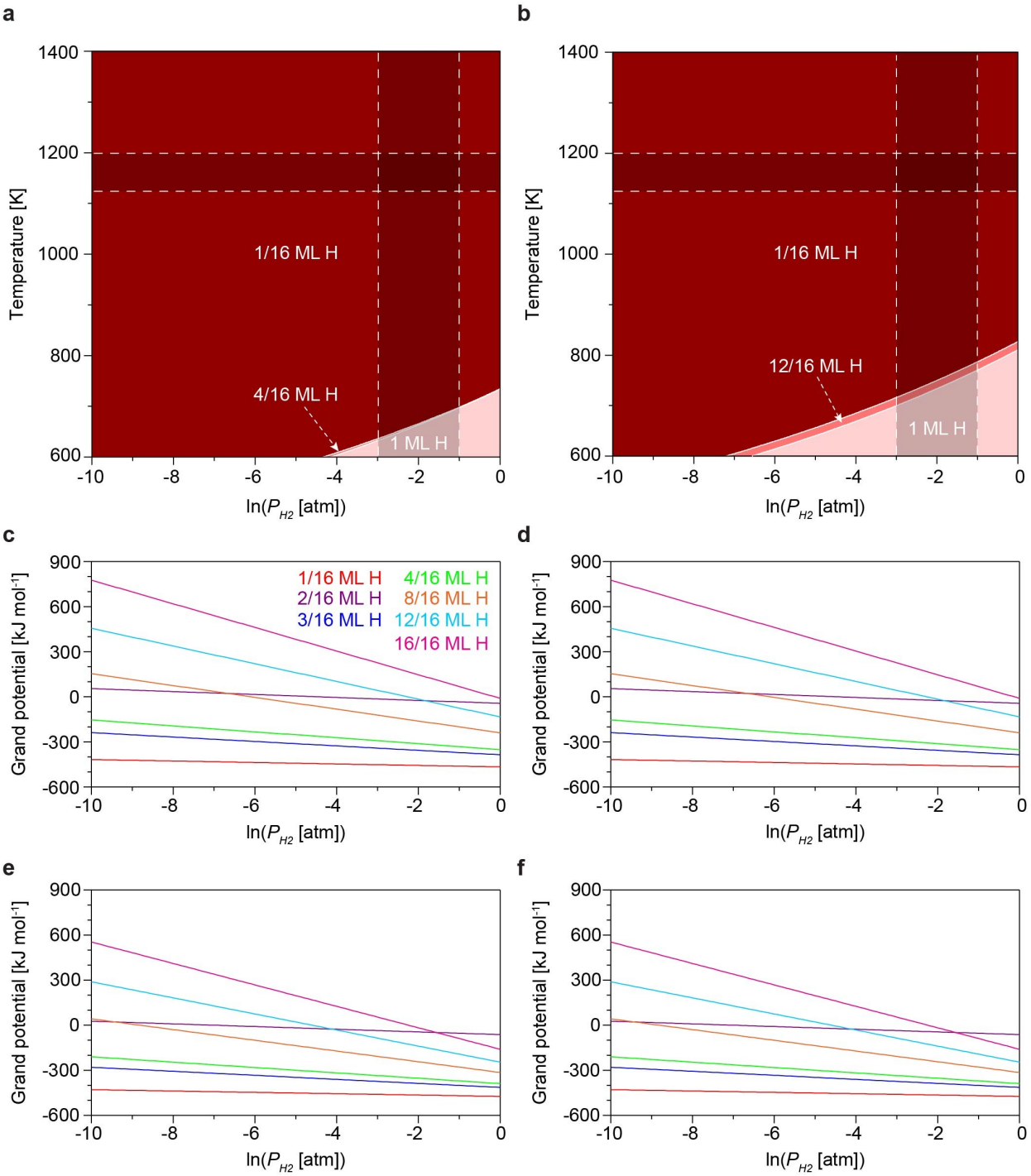

Fig. S10. DFT calculations of H coverage on Ge(001)-0°. (a,b) Thermodynamic phase diagram plotted against temperature and P_{H_2} using the strained (a) and relaxed (b) Ge lattice. Regions of stability are shown for Ge surfaces with 1/16th, 4/16th, and 1 ML of H (a) and 1/16th, 12/16th, and 1 ML of H (b). Shaded regions indicate a range of temperatures and P_{H_2} at which ribbons have been grown.[11] (c-f) Cutouts of the phase diagrams in a,b, plotting grand potential for 1/16th (red), 2/16th (purple), 3/16th (blue), 4/16th (green), 8/16th (orange), 12/16th (cyan), and 1 ML (magenta) of H versus P_{H_2} at 1183 K (c,d) and 1073 K (e,f) using the strained (c,e) and relaxed (d,f) Ge lattice.

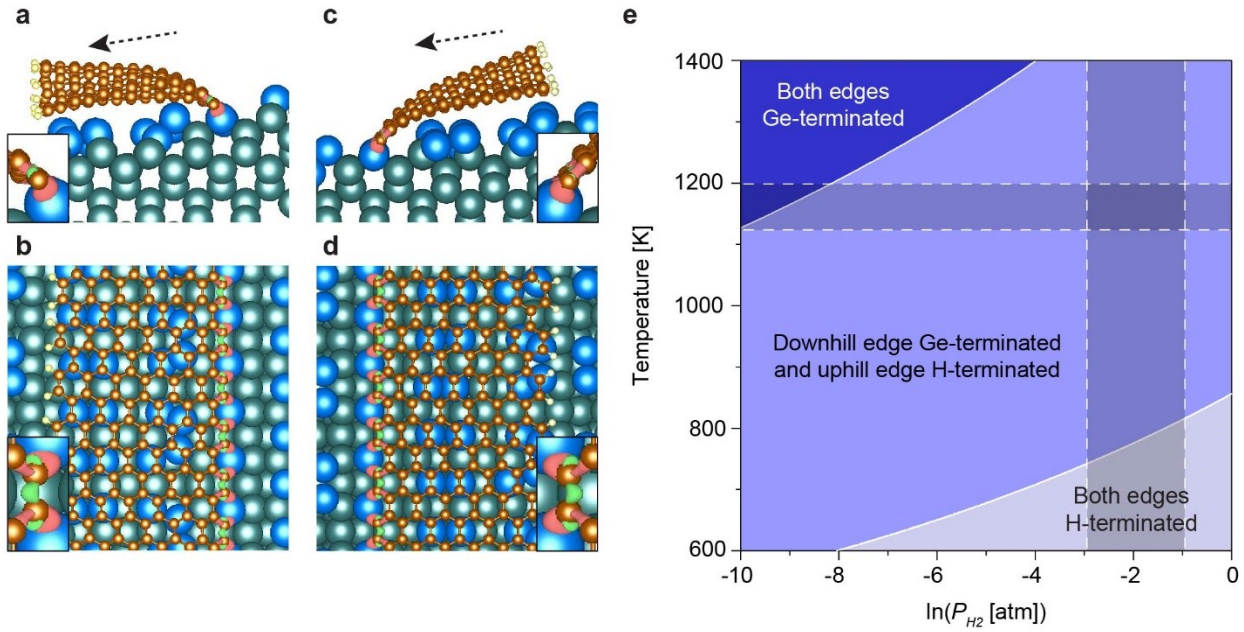

Fig. S11. DFT calculations of graphene nanoribbons on Ge(001)-9°. (a-d) Side view (a,c) and top view (b,d) of the minimum-energy structure in which the uphill (downhill) edge is not (is) terminated by H (a,b) and vice versa (c,d). Charge density isosurfaces (insets) show regions of increased (red) and decreased (green) electron density upon ribbon adsorption onto Ge(001)-9º. Green, blue, orange, and white atoms are Ge (saturated, bulk), Ge (unsaturated, surface), C, and H, respectively, and dashed arrows point downhill. (e) Thermodynamic phase diagram plotted against temperature and P_{H_2}. Regions of stability are shown for ribbons with both edges pinned, only the downhill edge pinned, and both edges unpinned. P_{CH_4} is 0.0067 atm. Shaded regions indicate a range of temperatures and P_{H_2} at which ribbons have been grown.[11] Results in a-e are calculated using the relaxed Ge lattice. Results for strained Ge are shown in Fig. 5.

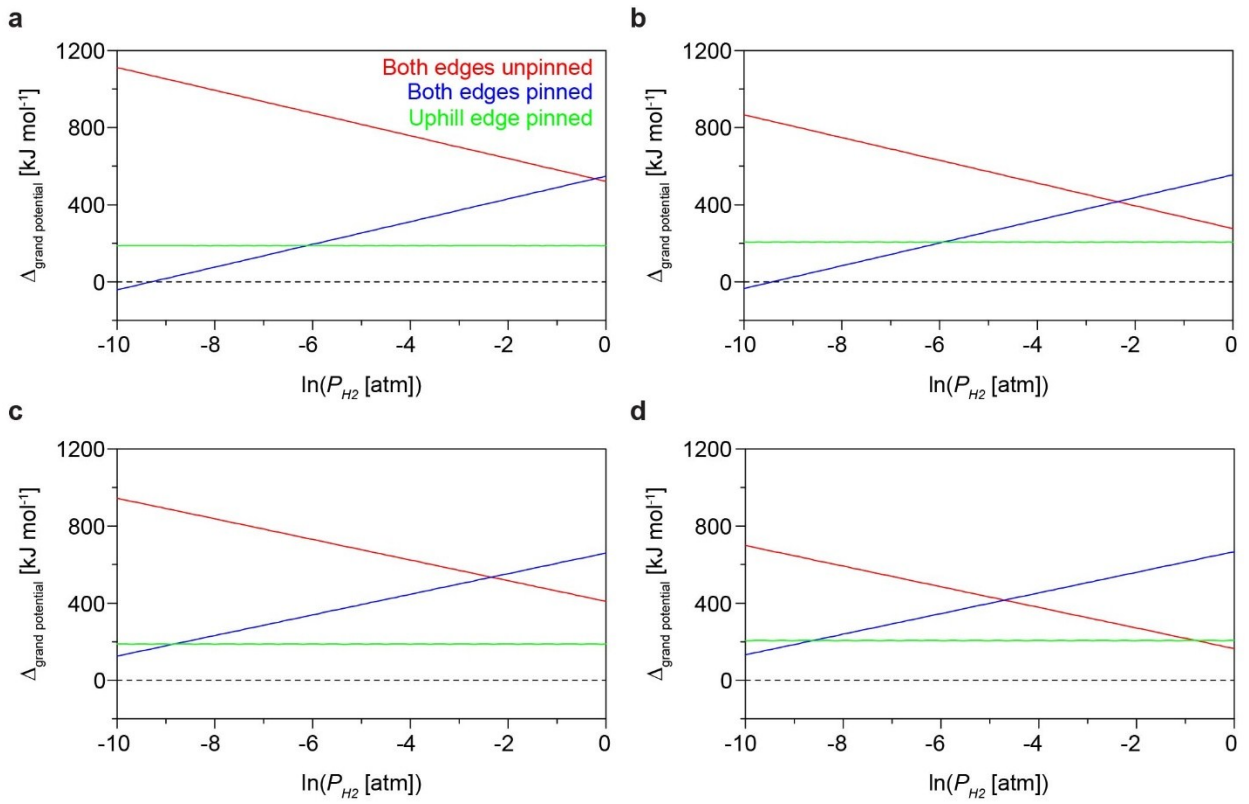

Fig. S12. DFT grand potential of nanoribbons on Ge(001)-9°. Cutouts of the phase diagrams in Fig. 5e and Fig. S11e, plotting the difference in grand potential between a ribbon with its downhill edge pinned and a ribbon with both edges unpinned (red), both edges pinned (blue), and only the uphill edge pinned (green) versus P_{H_2} at 1183 K (a,b) and 1073 K (c,d) using the strained (a,c) and relaxed (b,d) Ge lattice.

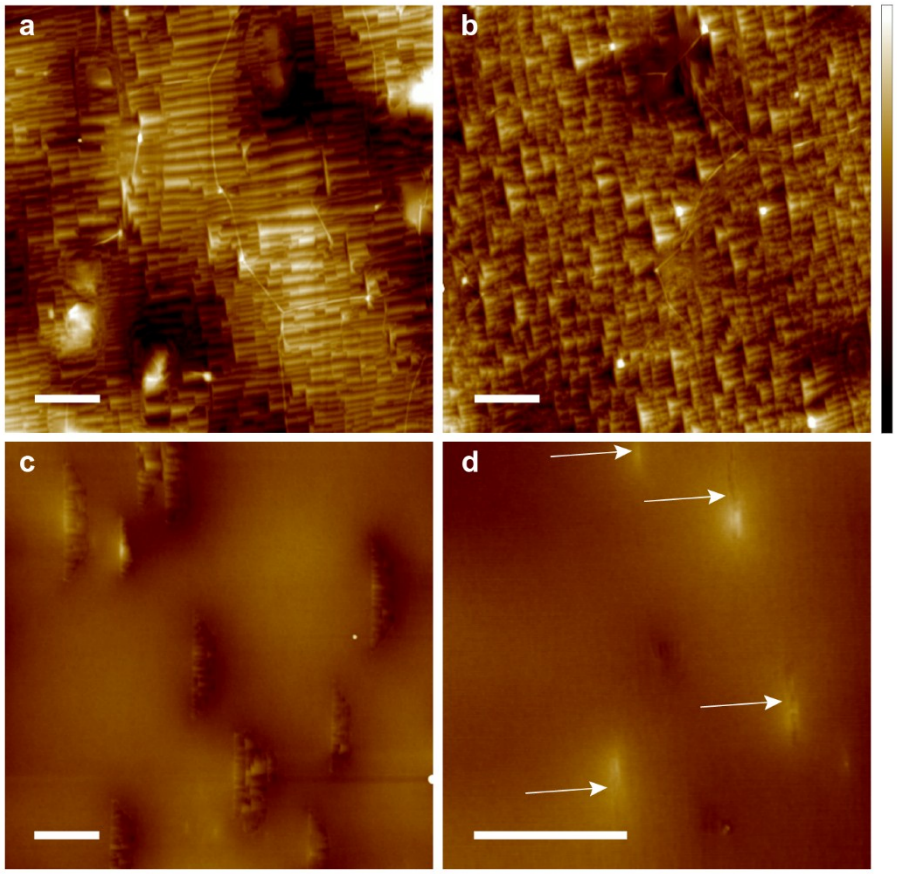

Fig. S13. AFM of graphene on Ge(001)-6° and Ge(001)-9°. (a-d) AFM images of continuous graphene films (a,b) and isolated graphene islands (c,d) grown on Ge(001)-6° (a) and Ge(001)-9° (b-d), in which the Ge surface below graphene is nanofaceted. The faceting of Ge is selective and only occurs below graphene, as shown in Fig. S13c. Furthermore, the facet angle is relatively shallow below narrow ribbons (Fig. S13d and Fig. 4c,d) and only becomes steeper as the ribbons grow wider (Fig. S13c) and eventually merge to form a continuous graphene film (Fig. S13b). Scale bars are 500 nm. Height scale is 20 nm. Arrows in d highlight the position of graphene ribbons.

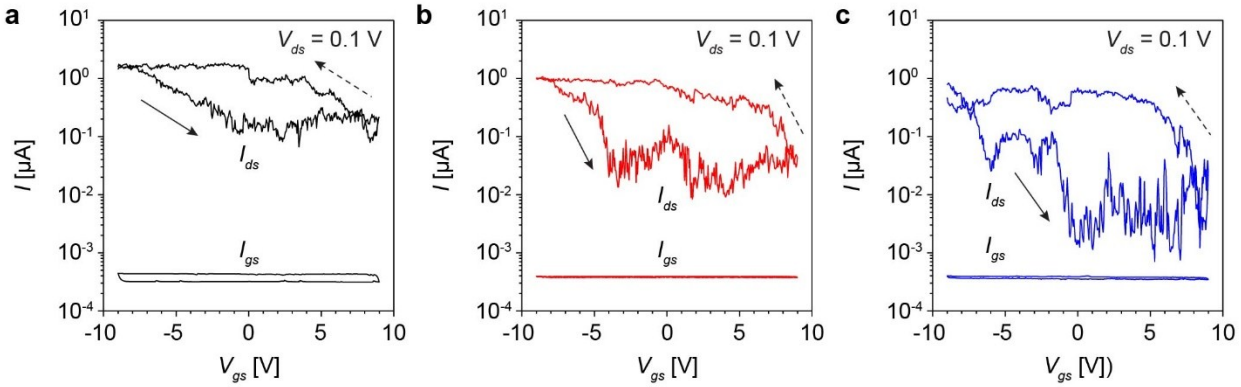

Fig. S14. Charge transport of nanoribbons grown on Ge(001)-9°. (a-c) Plot of I_{ds} (top curve) and I_{gs} (bottom curve) *versus* V_{gs} for three nanoribbons at V_{ds} of 0.1 V, corresponding to the I_{ds} *versus* V_{gs} curves with the same color in Fig. 6b,c.

Table S1. Summary of growth conditions. Conditions used in this work, including temperature (*T*), anneal time (t_{anneal}), growth time (t_{growth}), Ar flux (*Ar*), H_2 flux (H_2), and CH_4 flux (CH_4). For each synthesis, the same temperature, Ar flux, and H_2 flux are used for the anneal and growth steps.

Fig.	*T* [°C]	t_{anneal} [min]	t_{growth} [h]	*Ar* [sccm]	H_2 [sccm]	CH_4 [sccm]
1d,e,f	910	30	1.5	200	100	4.6
1g,h,i,j	910	60	2	200	100	2.8
2a	910	45	9	200	100	2.0
2b,e,h	910	30	1.5	200	100	4.6
2c,f,i	910	30	0.42	210	90	5.7
2d,g	910	15	6	200	100	2.0
3a,b	910	10	2	200	100	2.8
3c,d	910	30	1.5	200	100	4.6
4b	910	10	2.5	200	100	2.0
4c,d	910	0	0.67	200	100	1.7
6	910	~5	2	200	100	2.0
S1	910	60	2	200	100	2.8
S2b	910	10	0.33	200	100	4.6
S2c	910	20	0.67	200	100	4.6
S2d	910	60	1.5	200	100	4.6
S2e	910	10	0.75	200	100	2.8
S2f	910	30	2	200	100	2.8
S2g	910	45	2	200	100	2.8
S3	910	60	40	200	100	2.0
S3	910	60	18	200	100	2.8
S3	910	60	9	200	100	4.6
S3	910	60	2	210	90	5.7
S7	910	45	1.5	200	100	4.6
S8	910	45	1.5	200	100	4.6
S9	910	10	2	200	100	2.8
S13c	910	30	1.5	200	100	4.6
S13d	910	15	6	200	100	2.0
S14	910	~5	2	200	100	2.0

Supplementary information references

1. P. E. Blochl, *Phys. Rev. B*, 1994, **50**, 17953-17979.
2. G. Kresse and D. Joubert, *Phys. Rev. B*, 1999, **59**, 1758-1775.
3. G. Kresse and J. Furthmuller, *Comput. Mater. Sci.*, 1996, **6**, 15-50.
4. G. Kresse and J. Furthmuller, *Phys. Rev. B*, 1996, **54**, 11169-11186.
5. J. P. Perdew, K. Burke and M. Ernzerhof, *Phys. Rev. Lett.*, 1996, **77**, 3865-3868.
6. S. Grimme, *J. Comput. Chem.*, 2006, **27**, 1787-1799.
7. H. J. Monkhorst and J. D. Pack, *Phys. Rev. B*, 1976, **13**, 5188-5192.
8. K. Reuter and M. Scheffler, *Phys. Rev. B*, 2002, **65**, 035406.
9. J. Greeley, J. K. Norskov and M. Mavrikakis, *Annu. Rev. Phys. Chem.*, 2002, **53**, 319-348.

10. R. D. Johnson III, NIST Computational Chemistry Comparison and Benchmark Database, http://cccbdb.nist.gov.
11. R. M. Jacobberger, B. Kiraly, M. Fortin-Deschenes, P. L. Levesque, K. M. McElhinny, G. J. Brady, R. R. Delgado, S. S. Roy, A. Mannix, M. G. Lagally, P. G. Evans, P. Desjardins, R. Martel, M. C. Hersam, N. P. Guisinger and M. S. Arnold, *Nat. Commun.*, 2015, **6**, 8006.
12. V. I. Artyukhov, Y. Y. Liu and B. I. Yakobson, *Proc. Natl. Acad. Sci.*, 2012, **109**, 15136-15140.